

Measurements of Enhanced Turbulence in Short Wind-Induced Water Waves

Frank Hering¹, Dietmar Wierzimok^{1*}, and Bernd Jähne²

¹Institute for Environmental Physics, University of Heidelberg
Im Neuenheimer Feld 366, D-69120 Heidelberg, Germany
email: fhering@davinci.uphys.uni-heidelberg.de

²Scripps Institution of Oceanography, Physical Oceanography Res. Div.
La Jolla, CA 92093-0230, USA
email: bjaehne@ucsd.edu

Abstract

Particle Tracking Velocimetry was used to study turbulence beneath short wind-induced water-waves at the circular wind-wave facility of the Institute for Environmental Physics. Recording image sequences at up to 200 Hz allow an extensive study of the flow field. An automatic tracking algorithm was developed for the evaluation of the trajectories. Monte Carlo simulations show that Lagrangian flow field measurements offer an ideal approach to the study of drift profiles (mass transport) in the turbulent wave region. Also bulk velocity and surface velocities can be calculated. A measure for the turbulence was gained by the calculation of the friction velocity profile by correlating horizontal and vertical velocity components (eddy correlation technique).

1 Introduction

A *particle tracking* technique working with a high particle concentration for the measurement of flow fields beneath water waves was used. It features a 1-4 cm thick light sheet parallel to the main wave propagation direction so that the seeding particles stay long enough in the illuminated area to enable tracking over several wave periods (Figure 1). An area of $10.0 \times 10.0 \text{ cm}^2$ is observed by a CCD camera (Dalsa CA-D1-0256) with up to 200 images/s (Figure 2). An automatic tracking algorithm was developed allowing particles to be individually tracked over more than 400 images at particle concentrations up to 800 particles/image. As a result both the Lagrangian and the Eulerian vector field is measured. Details on technique and algorithms are reported by *Hering et al.* [1995]. This paper describes the appliance of *PTV* to the study of turbulence beneath short wind-Induced water waves. In section 2 various Monte Carlo simulations show, that mean properties of a flow (such as drift or friction velocity) can more easily and accurately be extracted close to the wavy free water surface from the Lagrangian flow

*Now affiliated to IBM Research Center Heidelberg

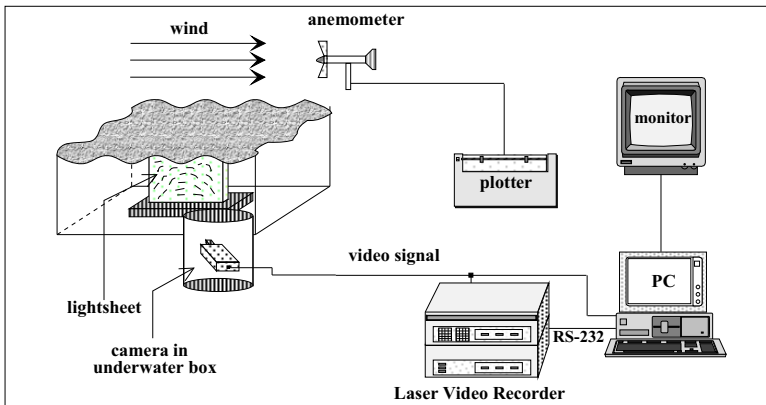


Figure 1: Scheme of the optical instruments used for flow visualization: A camera in an underwater box is looking perpendicular on a light sheet, illuminating seeding particles.

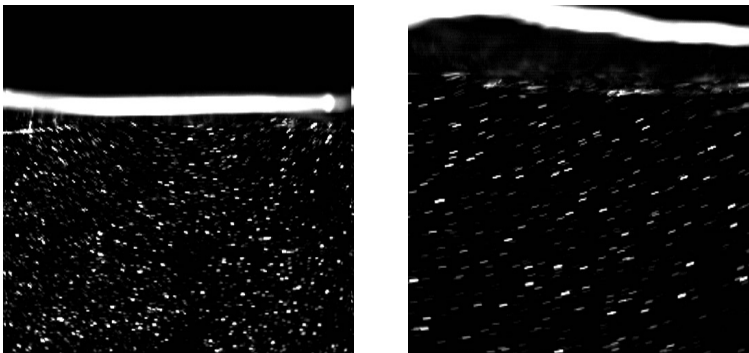


Figure 2: Seeding particles at a wind speed of 4.2 m/s (left) and 6.4 m/s (right) beneath the water surface in a light sheet illumination. Due to the exposure time of the camera particles in motion are visualized as streaks.

field, than from the Eulerian flow field. These simulations therefore form the basis for the resulting drift- and friction velocity computations (section 3).

2 A Study of the Eulerian vs. the Lagrangian Approach to the Calculation of Mean Properties of a Flow

The basic idea of the following *Monte Carlo simulations*, is to simulate the flow field with certain properties (such as a drift velocity) according to a model at various random grid points in space and time. These properties are then reextracted from the flow field, and the dependency of validity of

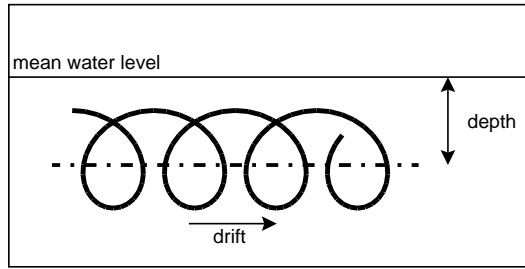


Figure 3: In contrast to point measurements (Eulerian), the exact location of the wavy water surface, is not required to be known if trajectories are measured (Lagrangian), as the mean height is calculated for each trajectory. The mean height of the trajectory in respect to the mean water level is calculated (see text).

the extraction on various parameters (such as the number of particles being tracked) is measured. Especial attention is directed to the problem of the moving free water surface, which may lead to an averaging at wrong heights (Figure 3). Eulerian measurements always require the simultaneous measurement of wave elevation and velocity to separate random orbital motions out of a random fluctuating motion [Thais and Magnaudet, 1995].

2.1 The Calculation of the Drift Velocity Profile

The information from the PTV is used for the study of momentum transport near the free boundary layer. Two approaches exist for calculating drift velocities, one using the *Eulerian flow field* data the other the *Lagrangian trajectory* information. The drift velocity is gained from the Eulerian flow field, by dividing the depth beneath the mean water level into a number of bins: By integrating over all vectors of a height bin the mean Eulerian drift $u_e(z)$ is gained:

$$u_e(z) = \frac{1}{t_1 - t_0} \int_{t_0}^{t_1} u_x(z) dt, \quad \text{for all vectors in that bin,} \quad (1)$$

$t_1 - t_0$ being the sequence length of the observation.

In contrast the drift velocity $u_l(z)$ is gained from the Lagrangian trajectory data, by integrating over all vectors belonging exactly to **same** trajectory. In addition the mean depth is calculated as the reference depth z' . Concluding from this data the drift is the mean of all previously calculated drift values assigned to each trajectory belonging to a depth bin:

$$u_l(z') = \frac{1}{n} \sum_{i=1}^n \frac{1}{t_{i0} - t_{i1}} \int_{t_{i0}}^{t_{i1}} u_x(z) dt, \quad \text{for all trajectories in that bin,} \quad (2)$$

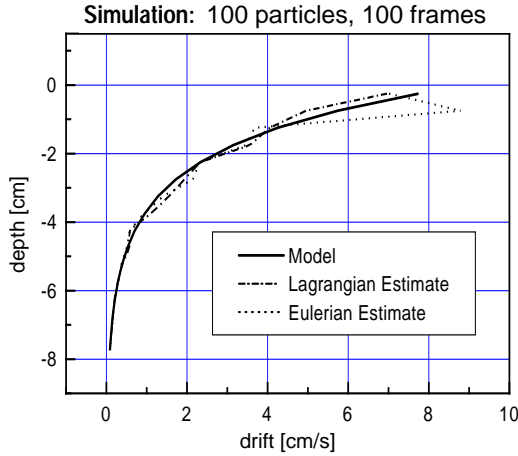


Figure 4: Drift velocity curves reconstructed from simulated flow fields (100 particles tracked over 100 image frames) by via Eulerian and Lagrangian averaging. Especially close to the water surface the Eulerian approach shows poorer results.

n being the number of trajectories in the height bin and $t_{i0} - t_{i1}$ the length of the i -th trajectory. The summation goes over all n trajectories in a depth bin.

Extensive Monte Carlo simulations have been undertaken to verify the errors on the velocity profile from the Eulerian respectively the Lagrangian averaging. A vector field generated at random grid points was simulated by:

$$\begin{aligned} u(x, z, t) &= A_0 e^{kz} \sin(kx - \omega t) + u_d(z) \\ v(x, z, t) &= A_0 e^{kz} \cos(kx - \omega t), \end{aligned} \quad (3)$$

A_0 being the amplitude of the wave, k the wave number, ω the frequency, and u_d the drift velocity profile function. It was therefore assumed that no Stokes drift is present and as a consequence Lagrangian and Eulerian drift velocities are identical.

Hence the Eulerian and Lagrangian vector field is known. The Eulerian drift velocity can then be reconstructed via eq. 1, the Lagrangian via eq. 2 and then compared to the input $u_d(z)$. The effect of various parameters, like particle density, sequence length, frequency of the wave, maximum drift etc. on the velocity profile can be studied. Figure 5 shows the effect of the number of trackable particles (particle density) and the period over which the particles are tracked (image sequence length) on the velocity profile. As measure of confidence a normalized χ^2 -function was chosen and plotted in

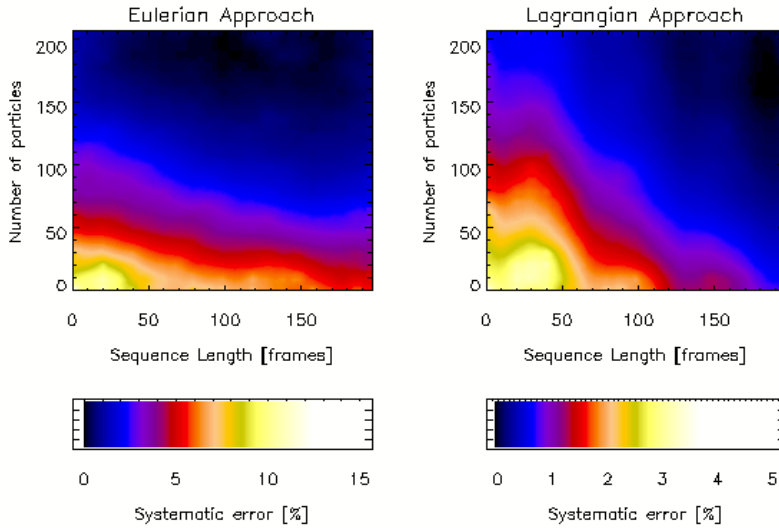


Figure 5: Monte Carlo simulation: The effect of particle density and image sequence length on the velocity profile calculations. (For color figure, see Plate 9.)

the figures:

$$\chi^2 = \sum_{z=1}^n \frac{(u_d(z) - u_{el})^2}{n}, \quad (4)$$

n , being the number of bins of the Eulerian, or respectively Lagrangian horizontal velocity component u_{el} .

Especially at low particle concentrations and short image sequences, the Lagrangian approach yields 2-3 times better results than the Eulerian. This is not very surprising as in this approach an additional information, namely the trajectorial data of a particle path, is taken into account. In addition the effect of the moving water surface much more important in the Eulerian reconstruction of the drift (Figure 4).

2.2 The Calculation of the Turbulent Reynolds Stress

To study the transport near the interface by fluctuating velocity the flow field is commonly represented in the form:

$$\vec{u} = \langle \vec{u} \rangle + \vec{u}', \quad (5)$$

$\langle \vec{u} \rangle$ being the average of the velocity over the time and \vec{u}' the deviation from the average. The contributions of the fluctuating velocities to the momentum flux form the *Reynolds stress tensor* τ_{ij} :

$$\tau_{ij} = -\rho \overline{v'_i v'_j}, \quad (6)$$

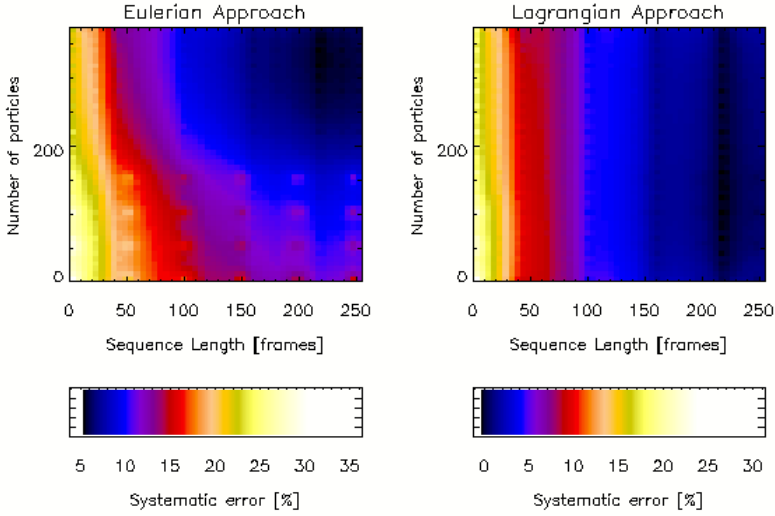


Figure 6: Monte Carlo simulation: The effect of particle density and image sequence length on the Reynolds stress calculation of 2 Hz wave. (For color figure, see Plate 10.)

v'_j and v'_j being the fluctuating velocity components of \vec{u}' . Of special importance for *friction velocity* calculations is the correlation of horizontal and vertical velocity fluctuations. The Monte Carlo simulations focuses on the question, whether the orbital movement beneath the water surface contributes significantly to the calculation of the stress component. For a monochromatic wave the additional offset to the stress component can be computed by integrating over a period T of the orbital wave motion and assuming no horizontal and vertical drift:

$$\begin{aligned}
 \overline{u'_x u'_z} &= \frac{1}{T} \int_0^T u'_x u'_z dt & (7) \\
 &= \frac{1}{T} \int_0^T A(z) \sin(kx - \omega t) B(z) \cos(kx - \omega t) dt \\
 &= \frac{A(z)B(z)}{T} \sin(2kx) \int_0^T [\cos(2\omega t) - \sin(2\omega t)] dt \\
 &= 0.
 \end{aligned}$$

Therefore when integrating $u'_x u'_z$ over one wave period no additional offset to the friction velocity computation is expected. When integrating over t , and t not being the wave period T the offset τ_{off} is of the order:

$$\tau_{off} = \mathcal{O}\left(\frac{A(z)B(z)T}{t}\right) \text{ assuming } t \gg T; \quad (8)$$

a long integration time (in comparison to the period of the wave) therefore

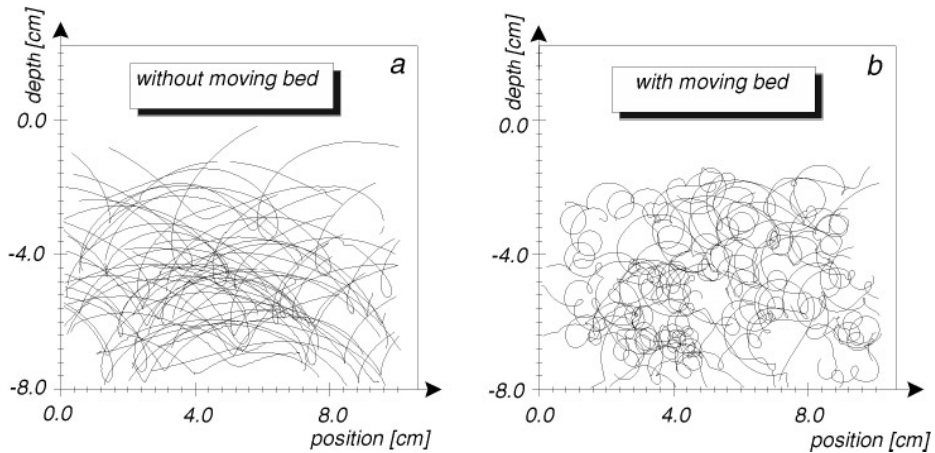


Figure 7: Trajectories of wind induced water waves without (a) and with (b) moving bed.

yields a neglectable offset. The effects of integration time (\equiv observation length), particle density, Eulerian and Lagrangian averaging were studied in a Monte Carlo simulation. As in the previous drift reconstruction the flow field was modelled using equation 3 at random observation points. The stress component was computed and then compared to the expected value (Eq. 7). Figure 6 shows the effect of the number of trackable particles (particle density) and the period over which the particles are tracked on the stress computation. The Lagrangian averaging approach yields superior results to the Eulerian as no dependency on particle density is found.

2.3 Results: PTV Beneath Water Waves

Figure 7 shows two typical trajectories measured at the circular wind/wave facility in Heidelberg. The wind wave flume was equipped with a moving bed installed at the bottom of the flume, moving against the wind induced currents. With this feature the main horizontal drift velocity can be reduced significantly. Particles stay longer in the light sheet, thus enabling the measurement of longer particle trajectories (Figure 7b). After now having studied the influences on the computation of drift profiles, the curves were calculated for various conditions at circular channel in Heidelberg. The wind speed was varied between 4–6 m/s and the fetch between 3–6 m. The fetch was limited by putting a 2 m long bubble foil on the water surface.

Figure 8 shows typical drift profiles for 5.2 m fetch at three different wind speeds. The observed trajectories ($x(t), z(t)$) were then used for a radius estimation (Figure 8d). As a first step *natural cubic splines* $S_x(t)$ and $S_z(t)$

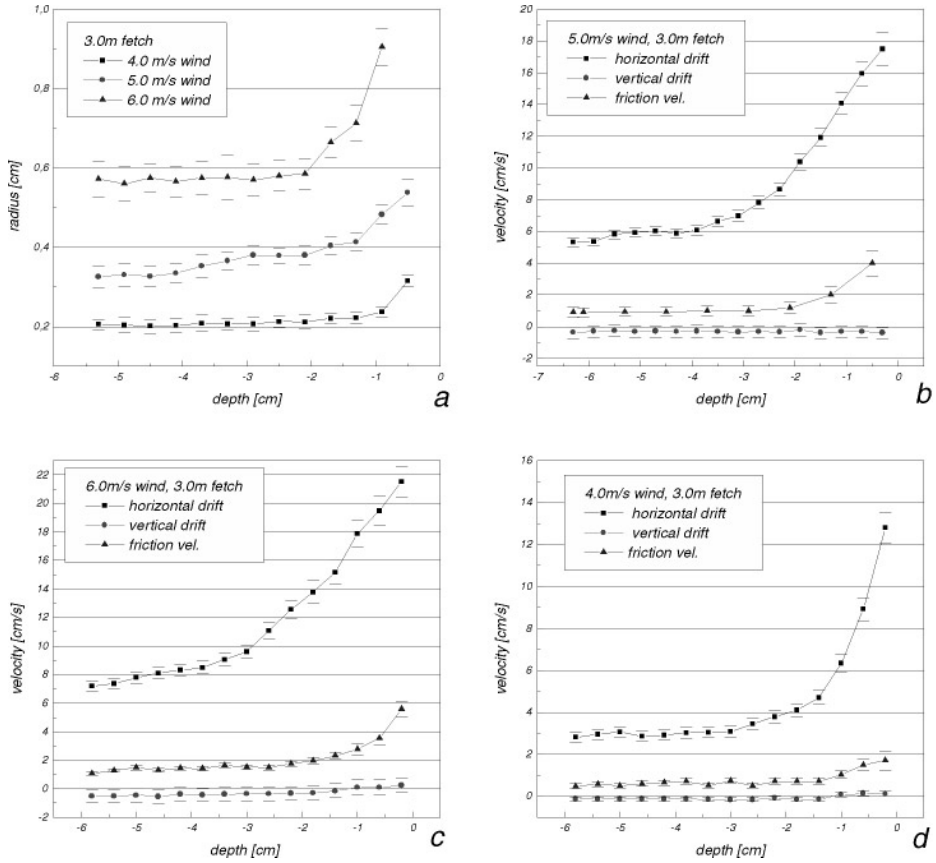


Figure 8: Horizontal and vertical drift velocities and turbulent friction velocity at three different wind speeds (a-c). Dependency of orbital radius on depth (d).

were fitted to the trajectory for all $t \in \{t_i, t_{i+1}\}$:

$$\begin{pmatrix} S_x^i(t) \\ S_z^i(t) \end{pmatrix} \equiv \begin{pmatrix} a_i + b_i(t - t_i) + c_i(t - t_i)^2 + d_i(t - t_i)^3 \\ a'_i + b'_i(t - t_i) + c'_i(t - t_i)^2 + d'_i(t - t_i)^3 \end{pmatrix} \approx \begin{pmatrix} x(t) \\ z(t) \end{pmatrix}. \quad (9)$$

The big advantage of the spline interpolation is that immediately the first and second temporal derivatives of $x(t)$ and respectively $z(t)$ are known. With this input the radius R can be computed for each trajectory:

$$R = \frac{(\mathcal{E}^2 + \mathcal{Z}^2)^{(3/2)}}{\mathcal{E}\ddot{z} - \ddot{x}\mathcal{E}}. \quad (10)$$

In addition an eddy correlation technique was used to determine the friction velocity and its profile. In the bulk of the water the viscous transport

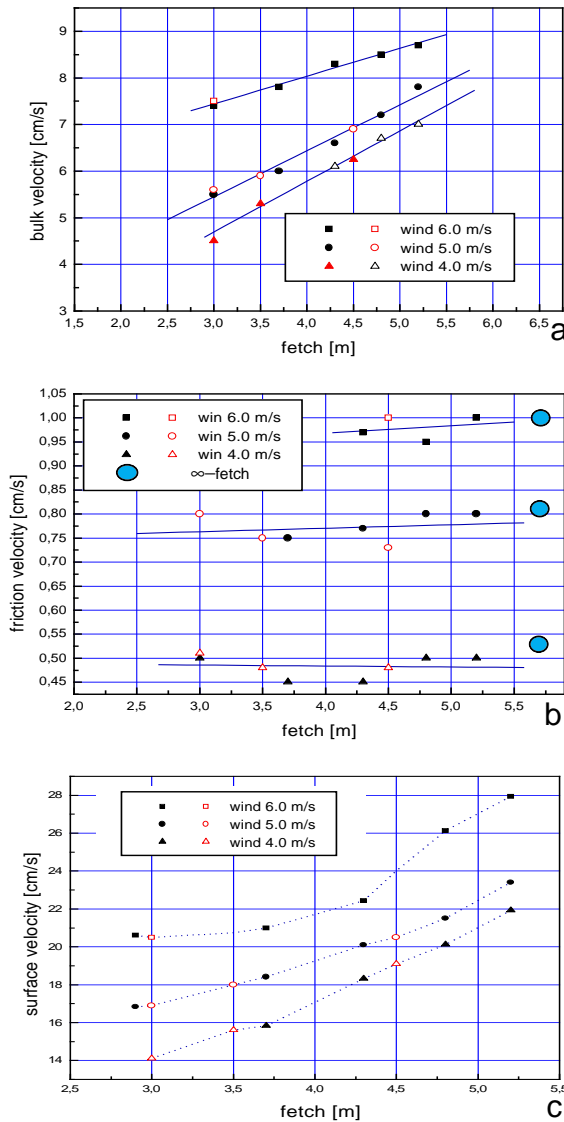


Figure 9: Dependency of bulk (a), friction velocity (b) and extrapolated surface velocity (c) on wind speed and fetch, measured at the circular in Heidelberg. Closed symbols denote measurements without the moving bed, the hollow ones with. Measurements of bulk and surface velocities with the moving bed have been corrected for the drift induced by the bed.

term can be neglected. The friction velocity profile $u_*(z)$ and its dependency on the water depth can therefore be directly determined by correlating the fluctuating velocities u'_x with u'_z , see (Figure 8). These profile curves show a very interesting behavior. On both sides of the interface the fluid are in turbulent motion and momentum is transported by turbulence. Upon reaching the boundary layer the interfacial turbulence is largely suppressed and molecular diffusion dominates the transport process. Modern boundary layer theories (see *Kraus and Businger* [1994]) predict a constant flux into the water bulk. Our measurements indicate however a significant enhancement of the friction velocity at the water surface (Figure 8). While the friction velocity is constant in the bulk, an abrupt enhancement of the Reynolds stress from the bulk towards the water surface up to a factor of 2-6 is observed. This suggests, that the orbital movement of wind waves significantly enhances turbulent dissipation near the water surface (Figure 8d).

Previously *Agrawal et al.* [1992] measured *enhanced dissipation* of kinetic energy beneath strongly breaking waves at the lake Ontario. They found an enhancement factor of 5-60. Our measurements now indicate that micro-scale wave breaking is sufficient to produce significant turbulence enhancement.

Figure 9 show the dependency of the bulk velocity and friction velocity (computed in the bulk) on wind speed and fetch. The bulk shows a linear increase with the fetch, the friction velocity however does not show this behavior, and remains nearly constant. In addition these values show lie in good agreement to previously measured friction velocity using a momentum balance method [*Jähne et al.*, 1997].

Acknowledgements

Financial support for this research from the National Science Foundation (OCE91 15994) and the German Science Foundation DFG (Wi 1029/2-1) is gratefully acknowledged.

References

- Agrawal, Y. C., Terray, E. A., Donelan, M. A., Hwang, P. A., Williams III, A. J., Drennan, W. M., Kahma, K. K., Kitaigarodskii, S. A., Enhanced Dissipation of kinetic energy beneath surface waves, *Nature*, 359, 219-220, 1992
- Hering, F., Wierzimok, D., Jähne, B., Particle Tracking and its Application of Turbulence beneath Water Waves, *submitted to Experiments in Fluids*, 1995
- Jähne, B., Münnich, K. O., Siegenthaler, U., Measurement of gas exchange and momentum transfer in a circular wind-water tunnel, *Tellus*, 31, 321-328, 1979
- Kraus, E.B., Businger, J.A., Atmosphere-Ocean Interaction, *Oxford university press*, 2nd edition, New York, 137-180, 1994
- Thais, L., Magnaudet, J., A triple decomposition of the fluctuating motion below laboratory wind water waves, *Journal of Geophysical Research*, 100, No. C1, 741-755, 1995